Chinese Journal of
POLYMER SCIENCE

RESEARCH ARTICLE

https://doi.org/10.1007/s10118-023-3004-5
Chinese J. Polym. Sci. **2023**, *41*, 1447–1461

Understanding Mass Dependence of Glass Formation in Ring Polymers

Xiang-Yu Song[a,b], Zhen-Yue Yang[a], Qi-Lu Yuan[a,b], Shang-Wei Li[a], Zi-Qiang Tang[a,b], Yue-Tong Dong[a,b], Shi-Chun Jiang[c*], and Wen-Sheng Xu[a,b*]

[a] *State Key Laboratory of Polymer Physics and Chemistry, Changchun Institute of Applied Chemistry, Chinese Academy of Sciences, Changchun 130022, China*
[b] *School of Applied Chemistry and Engineering, University of Science and Technology of China, Hefei 230026, China*
[c] *School of Materials Science and Engineering, Tianjin University, Tianjin 300072, China*

Abstract Having highly tunable molecular topology is one of the most important characteristics of polymers that provides these materials with a wide range of interesting and unique properties. In particular, ring polymers exhibit a number of properties that are markedly distinct from their linear counterparts. Here, we compare and contrast the glass formation of unknotted, nonconcatenated ring and linear polymer melts having variable molecular mass based on molecular dynamics simulations of a coarse-grained model. After revealing an unusual property in the structure of small rings, we discuss the mass dependence of the structural relaxation time determined from the self-intermediate scattering function over a wide range of temperatures in both ring and linear polymers. As a general trend, we find that the characteristic temperatures (*e.g.*, the glass transition temperature) and fragility of glass formation increase with increasing molecular mass in linear polymers, but the mass dependences of these properties are rather weak in the family of ring polymer models considered, in broad accord with experimental measurements. Importantly, we show that the glass formation of ring polymers can quantitatively be described by the string model, a model that is broadly consistent with the entropy theory of glass formation and that takes the mass of string-like clusters as a molecular realization of the abstract cooperatively rearranging regions. This opens the possibility of applying the configurational entropy-based theories to describe the glass formation of ring polymers, once the ring topology is taken into account.

Keywords Ring polymers; Glass formation; String model; Molecular dynamics simulation

Citation: Song, X. Y.; Yang, Z. Y.; Yuan, Q. L.; Li, S. W.; Tang, Z. Q.; Dong, Y. T.; Jiang, S. C.; Xu, W. S. Understanding mass dependence of glass formation in ring polymers. *Chinese J. Polym. Sci.* **2023**, *41*, 1447–1461.

INTRODUCTION

Ring polymers are a special type of macromolecules that lack free chain ends. The cyclic topology provides ring polymers with distinct conformational and viscoelastic properties in bulk, solution, and thin films when compared to linear or branched polymers.[1–25] In particular, ring polymers have been found to generally exhibit lower intrinsic viscosity, smaller hydrodynamic volume, higher density, higher glass transition temperature, and higher refractive index than their linear counterparts.[26] Consequently, ring polymers have become an attractive material for use in a variety of fields, such as drug delivery,[27–29] gene transfection,[30–33] energy storage devices,[34–36] *etc*. For instance, Karim and coworkers[36] recently showed that both the dielectric strength and capacitive energy density of polymer films can be enhanced by employing the cyclic topology because the free chains of linear polymers act as defect sites at which the dielectric breakdown can be initiated. Since cyclic biomacromolecules are commonly found in nature,[37–39] the study of ring polymers is also of great significance from a biological point of view. For a comprehensive discussion of the physical properties and potential applications of ring polymers, the reader is referred to the excellent review of Haque and Grayson[40] and the references therein.

The present work focuses on the glass formation of ring polymers, which is a long-standing problem in polymer science. The seminal arguments by Fox and Flory[41,42] relate the rate of segmental relaxation of polymers to the number of free chain ends of the molecule. This free-volume idea remains popular in the polymer science community[43,44] and is often invoked to rationalize the dependence of the glass transition temperature (T_g) of polymers on molecular mass. This picture implies that more free chain ends lead to a higher free volume or lower density and thus to a lower T_g, which is in general accord with the observations that T_g decreases with decreasing chain length in linear polymers in the low molecular mass regime. If the same arguments are applied to ring polymers, then one expects that T_g should not exhibit much variation as molecular mass is altered since ring polymers do not have any chain ends. This reasoning makes the study of ring polymers having variable molecular mass highly attractive in relation to an understanding of the fundamental nature of polymer glass formation. Accordingly, a number of

* Corresponding authors, E-mail: scjiang@tju.edu.cn (S.C.J.)
E-mail: wsxu@ciac.ac.cn (W.S.X.)

Special Issue: Theory and Simulation of Macromolecules
Received April 9, 2023; Accepted May 16, 2023; Published online July 5, 2023

experimental measurements have been made for the mass dependence of T_g of ring polymers. While this task might seem straightforward to be achieved at first sight, the experimental investigations over the past several decades have not led to a clear conclusion yet. Many studies report that T_g for ring polymers increases with increasing molecular mass,[2,40,45–54] while others claim that an increase in molecular mass leads to a reduction in T_g,[55–59] a picture that was discussed long ago by Di Marzio and Guttman[60] based on the entropy theory of polymer glass formation. More intriguingly, several studies have also found a non-monotonic variation of T_g with molecular mass in ring polymers.[58,59,61–63] The source of these conflicting reports has not been fully understood, but it has been widely appreciated that the contamination of linear polymers in a ring polymer melt could affect the measurements of T_g of a neat ring polymer melt, a point that has been carefully examined in the work of Tu and coworkers.[47] In this regard, computational simulations can offer insights that potentially help resolve the issues. Unfortunately, there have been few systematic computational studies of the mass dependence of glass formation of ring polymers.[56,57] Despite the disagreement on the general trend in the mass dependence of T_g of ring polymers, two conclusions appear to be quite clear when the results of ring polymers are compared to those of linear counterparts. More specifically, it has been generally observed that the T_g of ring polymers is higher than that of linear polymers having the same molecular mass and that the mass dependence of T_g is much weaker in ring polymers than in linear polymers. In addition, the difference between the T_g of ring and linear polymers is more pronounced at lower molecular masses, and as the molecular mass increases, the asymptotic values of T_g for ring polymers in the limit of large molecular mass tend to converge to those of linear polymers, regardless of the general trend in the variation of T_g with molecular mass.[2,40,46,47,50–55,58–62]

There are additional fundamental reasons to investigate the glass formation of ring polymers. From our own standpoint, ring polymers provide an ideal model system to test general ideas in the generalized entropy theory (GET) of polymer glass formation,[64–67] which combines the analytic lattice cluster theory (LCT) for the thermodynamics of polymer systems[68,69] and the Adam-Gibbs (AG) relation between the structural relaxation time and the configurational entropy.[70] The GET provides a predictive theory of the dependence of the structural relaxation time (τ_α) and other characteristic properties of glass formation on basic molecular structural parameters, *e.g.*, backbone and side-group rigidities, cohesive interaction strength, chain length, and monomer structure, and thermodynamic conditions, *e.g.*, temperature and pressure. Within this framework, molecular packing is predicted to be a dominant factor in determining both the T_g and fragility of glass-forming polymers, where the fragility characterizes the strength of the temperature dependence of τ_α. For instance, if the molecules can pack efficiently in space, these polymers exhibit a relatively weak T dependence of τ_α and are relatively strong glass-formers. In comparison, if the molecules pack less efficiently in space, these polymers have a stronger variation of τ_α with T and are more fragile glass-formers. It then comes as no surprise that ring polymers provide a perfect platform for testing the idea of packing efficiency because molecular packing can be tuned to a large extent, *e.g.*, by changing the molecular details of a ring polymer.[52,71,72] Indeed, Vargas-Lara *et al*.[71] showed that the glassy dynamics of low molecular mass ring polymer melts are greatly influenced by the knot complexity as quantified by the minimal crossing number, and the authors attribute their findings to alterations in molecular rigidity and packing, which are exactly the primary physical factors governing glass formation predicted by the GET. We also mention a related study based on dielectric spectroscopy and differential scanning calorimetry,[52] where the authors showed that T_g depends sensitively on the number of linkers within a cyclic polymer. This result is also in line with the general idea of the GET since molecular rigidity and packing are evidently varied as the number of linkers changes. It should also be emphasized that the dynamics of glass-forming liquids start to exhibit large complex changes at temperatures well above T_g and that highly fascinating physics has been revealed in the deep glassy state below T_g, so T_g just represents part of the story of glass formation. For instance, the temperature dependence of τ_α evidently provides much more insight into the nature of glass formation than T_g alone. Unfortunately, systematic studies have been rather limited concerning the temperature dependence of the dynamics and other characteristic properties of ring polymers.[52,56,63,73]

In the present work, we perform extensive molecular dynamics (MD) simulations of a coarse-grained model to address the essential phenomenology of structural and dynamic properties of ring polymers upon approaching T_g. As a first step towards a deep understanding of the glass formation of ring polymers, we focus on the glass formation of unknotted, nonconcatenated ring polymer melts having variable molecular mass. For purposes of comparison, we also perform corresponding simulations for linear polymer melts so that we can compare and contrast the glass formation of ring and linear polymer melts. Our analysis reveals a characteristic peak in the static structure factor of small rings that arises from the strong interchain correlations. We then discuss the mass dependence of τ_α determined from the self-intermediate scattering function over a wide range of T in both ring and linear polymers in an effort to discern the similarities and differences between the structural relaxation of ring and linear polymers. This is followed by determinations of the characteristic temperatures (*e.g.*, T_g) and fragility of glass formation. As a general trend, we find that the characteristic temperatures and fragility of glass formation increase with increasing molecular mass in linear polymers, but the mass dependences of these properties are rather weak in the family of ring polymer models considered, in broad accord with experimental measurements mentioned above. We also identify certain aspects that are not captured by the present coarse-grained model, and accordingly, we discuss how the model can be improved to describe the mass dependence of polymer glass formation. Going beyond the phenomenological analysis, we demonstrate that the glass formation of ring polymers can quantitatively be described by the string model,[65,74,75] a model that is broadly consistent with the entropy theory of glass formation and that takes the mass of string-like clusters as a molecular

realization of the abstract cooperatively rearranging regions (CRR) envisioned by AG.[70] While much work is required to incorporate the ring topology into the existing framework,[64–67] our work opens the possibility of applying the configurational entropy-based theories to describe the glass formation of ring polymers.

MODEL AND SIMULATION DETAILS

Model Description

We investigate the mass dependence of polymer glass formation based on a coarse-grained bead-spring model,[76,77] where each chain is composed of a number of connected statistical segments. The interactions of our polymer model are given by the following two potentials.

First, a truncated-and-shifted Lennard-Jones (LJ) potential is utilized to describe the excluded volume interactions between a pair of nonbonded beads,

$$U_{\mathrm{LJ}}(r) = 4\varepsilon\left[\left(\frac{\sigma}{r}\right)^{12} - \left(\frac{\sigma}{r}\right)^{6}\right] + C(r_{\mathrm{cut}}),\ r < r_{\mathrm{cut}} \quad (1)$$

where r denotes the distance between two beads and σ and ε set the length and energy scales of the system, respectively. The constant $C(r_{\mathrm{cut}})$ ensures that the U_{LJ} goes smoothly to zero at the truncation distance r_{cut}, which is chosen to be $r_{\mathrm{cut}} = 2.5\sigma$ so that attractive nonbonded interactions are included.

Second, bonded interactions between two neighboring beads along a polymer chain are modeled using the finitely extensible nonlinear elastic (FENE) potential,

$$U_{\mathrm{FENE}}(r) = -\frac{1}{2}k_{\mathrm{b}}R_0^2\ln\left[1 - \left(\frac{r}{R_0}\right)^2\right] + U_{\mathrm{WCA}} \quad (2)$$

where $k_{\mathrm{b}} = 30\ \varepsilon/\sigma^2$ and $R_0 = 1.5\ \sigma$. The first term of Eq. (2) is an attractive potential which extends to R_0 and the second term is the purely repulsive Weeks-Chandler-Andersen (WCA) potential,[78] which has the same form as Eq. (1), but with a cutoff distance of $r_{\mathrm{cut}} = 2^{1/6}\ \sigma$. With the parameters described above, the polymer chains have an equilibrium bond length of approximately 0.97 σ,[76] introducing a length scale that differs from the equilibrium distance of nonbonded beads governed by U_{LJ}. These two competing length scales allow for the formation of an amorphous glass at low temperatures.

In our polymer system, the chain length N of both ring and linear polymers varies from 3 to 20, and the number N_{c} of chains is adjusted to keep the total number of beads fixed approximately at N_{b}=8000. The lower limit of N=3 for chain length corresponds to a case where the ring topology can still be defined in the present coarse-grained model. A model with small values of N may not be considered as a polymer, but we include the results for these models to examine polymer glass formation over a broad range of molecular masses. The upper limit of N=20 for chain length lies in a mass range where the segmental properties of polymer melts do not change much with varying the chain length.

In the following, we describe all quantities and results obtained from our simulations in terms of standard reduced LJ units. All beads have the same mass m_{b}. Length, time, temperature and pressure are then measured in units of σ, τ, $\varepsilon/k_{\mathrm{B}}$, and ε/σ^3, respectively, where $\tau \equiv \sqrt{m_{\mathrm{b}}\sigma^2/\varepsilon}$. The Boltzmann constant is set to be k_{B}=1 for convenience, and this factor is explicitly included in some equations for the sake of clarity.

Simulation Details

The Large-scale Atomic/Molecular Massively Parallel Simulator (LAMMPS) molecular dynamics package[79,80] is utilized to perform MD simulations in three dimensions under periodic boundary conditions, and the equations of motion are integrated with a time step of $\Delta t = 0.005\ \tau$. To prepare an equilibrated polymer melt that is subsequently used for the study of glass formation, we run simulations in the *NPT* ensemble at a relatively high temperature of $T = 1.5\ \varepsilon/k_{\mathrm{B}}$ and a pressure of $P = 0.0\ \varepsilon/\sigma^3$, where a Nosé-Hoover thermostat and barostat are employed to maintain the temperature and pressure, respectively, as implemented in LAMMPS. These simulations are performed for at least $10^5\ \tau$, followed by a subsequent run of the same duration under the aforementioned thermodynamic conditions to determine the number density $\rho = N_{\mathrm{b}}/V$, where V is the volume of the simulation box. The polymer melt with the desired density is further equilibrated at the same T for at least $10^5\ \tau$ in the *NVT* ensemble, which is much longer than the longest relaxation time of the melt so that the proper equilibration of the polymer melt can be achieved.

The equilibrated melt is then cooled or heated at $P = 0.0\ \varepsilon/\sigma^3$ in the *NPT* ensemble with a rate of $10^{-4}\ \varepsilon/(k_{\mathrm{B}}\tau)$, allowing us to obtain the density as a function of T under constant pressure conditions. Specifically, both linear and ring polymer melts are cooled down to a temperature of $T = 0.2\ \varepsilon/k_{\mathrm{B}}$, a value that is typically much lower than the glass transition temperature T_{g}. This procedure provides us with rough estimates of T_{g} because the slope in the T dependence of thermodynamic properties, such as ρ and V, exhibits a noticeable change at a temperature near T_{g}. The present study focuses on a regime of T well above T_{g}, thereby avoiding the nonequilibrium phenomena in the glass state. Since we focus on the regime of T where equilibrium properties can be accessible to the present simulations, the lowest temperatures at which we can perform equilibrium simulations are generally much higher than $T = 0.2\ \varepsilon/k_{\mathrm{B}}$ and the specific values of these temperatures depend on the chain topology and the chain length. In particular, when the chain length N is increased from 3 to 20, the lowest T ranges from 0.39 $\varepsilon/k_{\mathrm{B}}$ to ~0.42 $\varepsilon/k_{\mathrm{B}}$ for the linear polymer melts and it remains fixed at 0.43 $\varepsilon/k_{\mathrm{B}}$ for the ring polymer melts. We then perform additional simulations for each T in the *NPT* ensemble to determine the number density more accurately using the configuration obtained from the cooling or heating process. This is followed by a further equilibration of the polymer melt with the desired density for each T in the *NVT* ensemble, which typically lasts over a period ranging from 10 times to 100 times longer than the segmental structural relaxation time. Relevant quantities and properties of interest are finally analyzed, as discussed below. This enables us to obtain reliable equilibrium data on the segmental level. It should be pointed out that the chain conformations on large length scales are not readily equilibrated at very low T due to the very long relaxation times of polymer chains. Hence, there could be nonequilibrium effects for the properties on large length scales.

RESULTS AND DISCUSSION

Structural Properties

We start by analyzing the variation of structural properties of polymer melts with molecular mass. While the structures of

linear polymer melts are not commonly discussed in the context of glass formation, the cyclic topology may lead to changes in structure that are relevant to the understanding of the segmental dynamics. We first focus on the static structure factor of the beads,

$$S(q) = \frac{1}{N_b}\left\langle \sum_{j=1}^{N_b}\sum_{k=1}^{N_b} \exp\left[-i\mathbf{q}\cdot(\mathbf{r}_j - \mathbf{r}_k)\right]\right\rangle \quad (3)$$

where i is the imaginary unit, $q = |\mathbf{q}|$ is the wave number, $\mathbf{r}_j$ represents the position of particle j, and the brackets $\langle\cdots\rangle$ denote the usual thermal average.

Fig. 1 displays the q dependence of $S(q)$ at a relatively high temperature of k_BT/ε = 1.50 and a low temperature of k_BT/ε=0.43 for ring and linear polymer melts. Upon a comparison between the ring and linear polymer melts in Figs. 1(a) and 1(b), our simulation results indicate that the primary peak of both systems at about q = 7.0 σ^{-1} exhibits a mild dependence on N. Intriguingly, we find a characteristic peak or shoulder at around q = 3 ~ 4 σ^{-1} in ring polymer melts with small N. This result suggests the existence of structural characteristics in small ring polymer melts, and below, we provide insight into this structural feature by analyzing the static correlations between the chain centers of mass.

We can provide insight into the characteristic peak of $S(q)$ in small rings by analyzing the interchain correlations. The dashed lines in Fig. 1 show the results of the static structure factor $S_{cm}(q)$ for the chain centers of mass. The computations of $S_{cm}(q)$ follow the same method as in Eq. (3) but with the bead positions replaced by the chain centers of mass and the bead number replaced by the chain number. The peaks in $S_{cm}(q)$ clearly indicate the presence of strong interchain correlations in small ring polymer melts. We also find that the peak magnitude becomes most pronounced for the ring polymer melt with N = 4 and progressively decreases with increasing N. It can naturally be expected that $S_{cm}(q)$ is completely featureless in the large N limit. Evidently, it is the strong interchain correlations that lead to the characteristic peak in $S(q)$. It should be noted that $S_{cm}(q)$ also displays a peak in linear polymer melts with small N (Fig. 1b), but the interchain correlations are likely not sufficiently strong to cause a pronounced feature in $S(q)$, in contrast to the small ring polymer melts.

Moreover, Fig. 1(c) indicates that the characteristic peak or shoulder in $S(q)$ is nearly invisible at low T. This trend can be expected since the compressibility of glass-forming materials tends to vanish upon approaching the glassy state,[81] an effect that suppresses the occurrence of structural features in the low q regime. We note in passing that the statistics become poorer at lower T in our results of $S(q)$ and $S_{cm}(q)$. This is due to the significant increase of τ_α upon lowing T so that the protocol based on the time averaging is less effective. This issue can be alleviated by extending the total simulation time and increasing the number of independent runs at low T. Nonetheless, the structural characteristics of $S_{cm}(q)$ are evident even at low T, as shown in Fig. 1(d).

A natural question then arises as to what causes the interchain correlations in small rings. The correlation hole effects

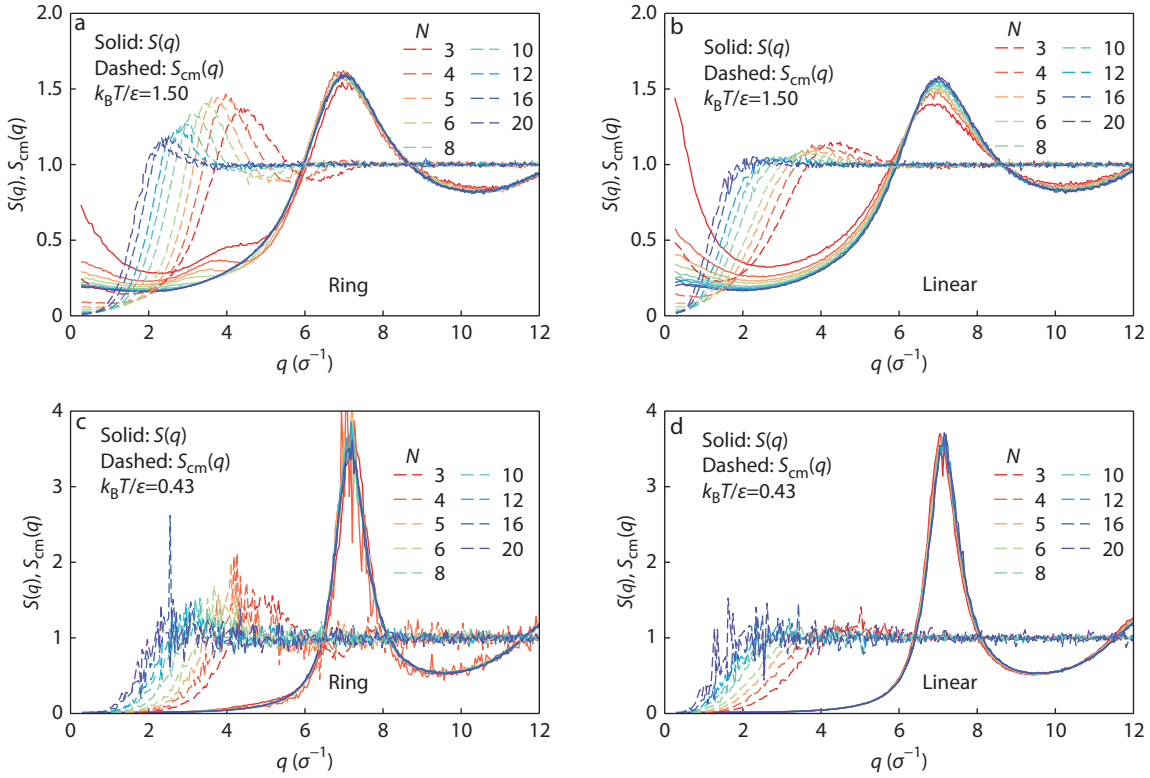

Fig. 1 Static structure factors $S(q)$ and $S_{cm}(q)$ for the beads and the chain centers of mass at a temperature of k_BT/ε=1.50 and 0.43 for polymer melts having variable chain length N, respectively. Panels (a) and (c) and (b) and (d) correspond to the results for ring and linear polymer melts, respectively. Solid and dashed lines correspond to $S(q)$ and $S_{cm}(q)$, respectively.

https://doi.org/10.1007/s10118-023-3004-5

might be a relevant factor in this context. The correlation hole has a size comparable with the overall chain size, giving rise to a characteristic feature in the single-chain static structure factor at the distance corresponding to the polymer coil radius, as discussed by de Gennes.[82] In more recent years, the correlation hole effects have been utilized to explain the non-Gaussian deviations of the form factor.[83,84] To check this possibility, we have examined $S(q)$ and $S_{cm}(q)$ versus qR_g (data not shown), where R_g is the chain radius of gyration. If the interchain correlations are caused by the correlation hole effects, the characteristic peak should appear at $qR_g \approx 1$, regardless of the chain length. However, our analysis indicates that the characteristic peak position of $S_{cm}(q)$ corresponds to a distance considerably smaller than the polymer coil radius and changes with varying the chain length. It is thus unlikely that the interchain correlations in small ring polymer melts are due to the correlation hole effects. The origin of the interchain correlations deserves a further study.

As a backdrop to frame our investigation of the dynamic properties of glass formation below, we further analyze the structures of our polymer model at a low temperature of $k_BT/\varepsilon = 0.43$, where dynamic heterogeneity is evident. Fig. 2 shows the center-of-mass radial distribution function, $g_{cm}(r)$, for both ring and linear polymers having variable N, which is calculated according to its standard definition,[85]

$$g_{cm}(r) = \frac{V}{N_c^2}\left\langle \sum_i^{N_c}\sum_{j\neq i}^{N_c}\delta(\mathbf{r}-\mathbf{r}_{cm,ij})\right\rangle \quad (4)$$

where $\mathbf{r}_{cm,ij}$ denotes the distance between the centers-of-mass of the i^{th} and j^{th} chains. As can be seen, $g_{cm}(r)$ for small ring polymer melts exhibit multiple peaks, and the ring polymer melt with N=4 appears to have the strongest interchain correlations, which have a dramatic influence on the dynamics, as discussed below. As N increases, $g_{cm}(r)$ for ring polymer melts becomes more featureless and is similar to that of linear polymer melts.

To further understand the structural features of small ring polymer melts, we also calculate the probability distribution function $P(\theta)$ of bond angle θ,

$$\theta = \cos^{-1}\left(\frac{\boldsymbol{b}_j\cdot\boldsymbol{b}_{j+1}}{|\boldsymbol{b}_j||\boldsymbol{b}_{j+1}|}\right) \quad (5)$$

where $\boldsymbol{b}_j = \boldsymbol{r}_j - \boldsymbol{r}_{j-1}$ represents the bond vector between adjacent particles j and $j-1$ on the polymer chain. As shown in Fig. 3, $P(\theta)$ for linear polymer melts is nearly independent of chain length. In sharp contrast, $P(\theta)$ for small ring polymer melts differs significantly from those having large N. More specifically, $P(\theta)$ for the ring polymer melt with N=3 exhibits a single peak with the peak position close to 2π/3, corresponding to an equilateral triangle chain conformation. In the case of N=4, $P(\theta)$ displays a double-peak distribution, with the peak positions being

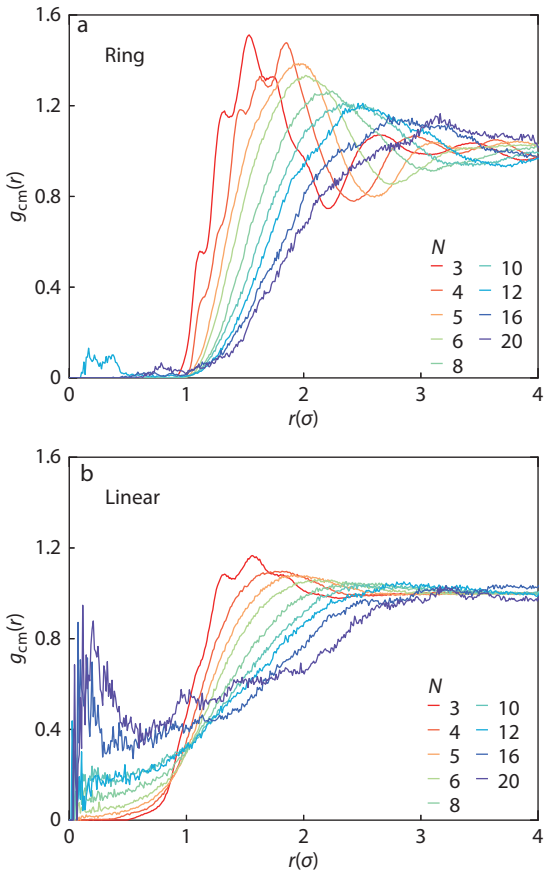

Fig. 2 Radial distribution function $g_{cm}(r)$ for the chain centers of mass at k_BT/ε=0.43 for polymer melts having variable N. Panels (a) and (b) correspond to the results for ring and linear polymer melts, respectively.

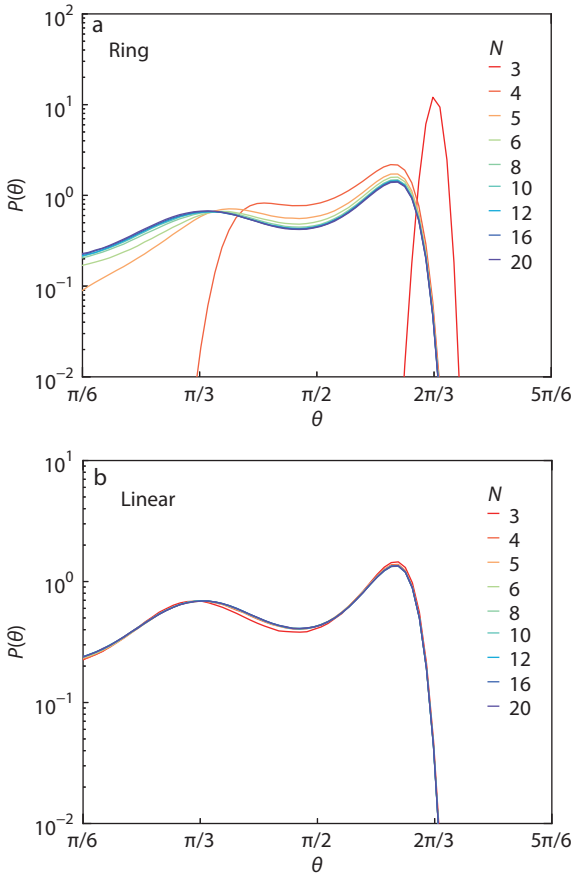

Fig. 3 Probability distribution function $P(\theta)$ of bond angle θ at k_BT/ε=0.43 for polymer melts having variable N. Panels (a) and (b) correspond to the results for ring and linear polymer melts, respectively.

https://doi.org/10.1007/s10118-023-3004-5

approximately symmetrical about π/2, indicating that the chain conformation adopts a rhombus shape. This is associated with the structural features revealed by $g_{cm}(r)$. As N increases, $P(\theta)$ gradually becomes uniform, exhibiting a similar distribution to that of linear polymer melts. Evidently, the topological constraint of the ring topology on chain conformation gradually weakens with increasing N.

Structural Relaxation Time

The structural relaxation time τ_α is a key quantity in the study of glass formation, from which the characteristic temperatures and fragility of glass formation can be determined. To investigate the influence of molecular mass on the relaxation of ring and linear polymer melts, we determine τ_α from the self-part of the intermediate scattering function,

$$F_s(q,t) = \frac{1}{N_b}\sum_{j=1}^{N_b} \exp\{-i\boldsymbol{q}\cdot[\boldsymbol{r}_j(t) - \boldsymbol{r}_j(0)]\} \quad (6)$$

where $\boldsymbol{r}_j(t)$ is the position of the j^{th} bead at time t. We choose the wave number to be $q = 7.0\ \sigma^{-1}$, which is close to the position of the primary peak of $S(q)$, so that we analyze the dynamics at the segmental length scale. We then define τ_α by the time where $F_s(q,t)$ decays to 0.2, following the previous works.[86–92]

Fig. 4 displays the t dependence of $F_s(q,t)$ at two different T for ring and linear polymer melts having variable N. It is observed that molecular mass has only a mild impact on the dynamics at high T in both ring and linear polymer melts. At low T, $F_s(q,t)$ for ring polymers do not change much with increasing N, except for N=4, while $F_s(q,t)$ for linear polymer melts shows a much stronger N dependence. As a typical feature of glass-forming liquids, the structural relaxation slows down drastically upon lowering T and the t dependence of $F_s(q,t)$ develops a two-step decay at low T. Here, the short-time β-relaxation reflects a fast inertial relaxation process that is prevalent at high T, which becomes progressively diminished by the onset of local caging in the liquid at lower T, where relaxation correspondingly becomes non-Arrhenius,[93] as discussed below. The long-time α-relaxation is strongly associated with the disintegration of dynamic clusters of caged particles.[94,95]

It is noteworthy that $F_s(q,t)$ for the ring polymer melt with N=4 exhibits an anomalous behavior at low T, as shown in Fig. 4(a), where the relaxation time cannot be obtained within the simulation time window. A further investigation reveals that this system cannot reach equilibrium in the NPT ensemble, as the volume of the simulation box varies even after a long simulation time. This issue is associated with the strong interchain correlations, as discussed earlier. For this reason, the results for the ring polymer melt with N=4 are excluded from the following discussion.

Fig. 5(a) summarizes our simulation data for τ_α as a function of $1/T$ for ring and linear polymer melts with various N. It is evident that τ_α increases dramatically upon cooling, a typical feature of glass-forming materials. In the high T regime, the T dependence of τ_α follows the Arrhenius equation, as anticipated from transition state theory (TST),[96,97]

$$\tau_\alpha = A_o \exp\left(\frac{\Delta H_o}{k_B T}\right) \quad (7)$$

where A_o is a prefactor and ΔH_o is the activation enthalpy. In Fig. 5(b), we confirm that the Arrhenius equation applies at high T in our polymer model having variable N. The simulation data for both ring and linear chains collapse onto a master curve in the high T Arrhenius regime. In the relatively low T regime, however, the T dependence of τ_α deviates from the Arrhenius behavior[98,99] and can typically be described by the Vogel-Fulcher-Tammann (VFT) equation,[100–102]

$$\tau_\alpha = \tau_o \exp\left(\frac{DT_0}{T - T_0}\right) \quad (8)$$

where τ_o is the high T limit of τ_α, D is a fragility index that quantifies the strength of the T dependence of τ_α, and T_0 is the hypothetical "ideal glass transition temperature"[64] at which τ_α extrapolates to infinity. Angell has emphasized that the parameters of the VFT equation are quite sensitive to the range of T chosen for the fits. The T range that can be reached in simulations is actually much higher than T_g, where τ_α only changes several orders of magnitude, making the estimations of D and T_0 highly uncertain.

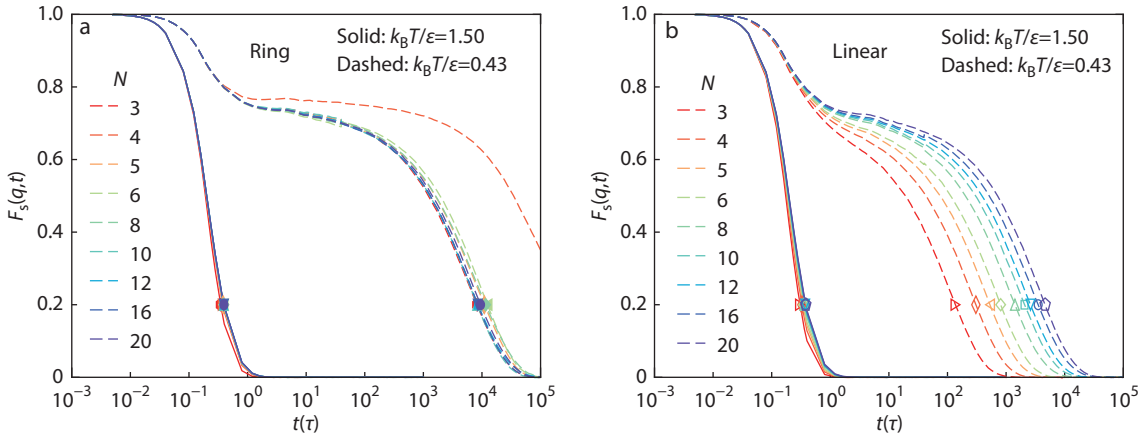

Fig. 4 Self-intermediate scattering function $F_s(q,t)$ as a function of time t at fixed T for polymer melts having variable N. Panels (a) and (b) correspond to the results for ring and linear polymer melts, respectively. Solid and dashed lines correspond to the results for k_BT/ε=1.50 and 0.43, respectively. Symbols indicate the positions where $F_s(q,t)$ decays to the value of 0.2, a condition that serves to define the structural relaxation time τ_α. The wave number is chosen to be $q = 7.0\ \sigma^{-1}$ in the present work. Notice the unusual behavior of the ring polymer melt with N=4 at k_BT/ε=0.43.

https://doi.org/10.1007/s10118-023-3004-5

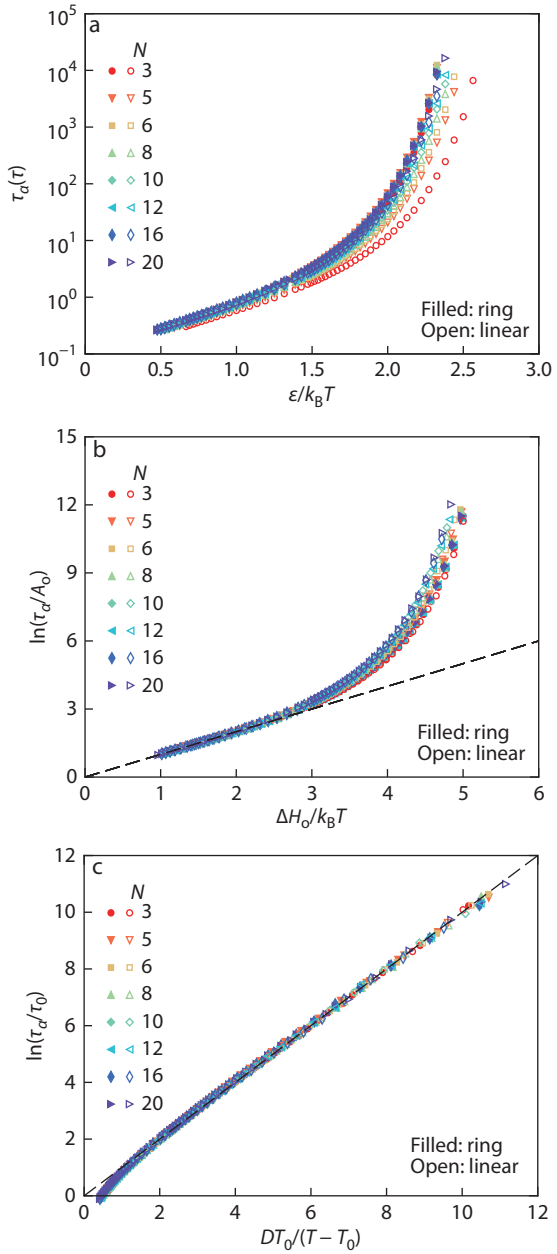

Fig. 5 (a) τ_α versus inverse temperature ε/k_BT for a range of N; (b) Data reduction of the T dependence of τ_α based on the Arrhenius equation. The dashed line indicates $\ln(\tau_\alpha/A_o) = \Delta H_o/k_BT$. (c) Data reduction of the T dependence of τ_α based on the VFT equation. The dashed line indicates $\ln(\tau_\alpha/\tau_o) = DT_0/(T-T_0)$. Filled and open symbols correspond to the results for ring and linear polymer melts, respectively.

We found that it is challenging to obtain reliable fitted results for variable N when all the three parameters (τ_o, T_0, and D) are allowed to vary simultaneously. Inspired by the previous work,[86,89,91] we fix τ_o at average values obtained by fitting the data for ring and linear polymer melts of all chain lengths, which are τ_o≈0.30 and τ_o≈0.28 for ring and linear polymer melts, respectively, while T_0 and D are treated as independent fitting parameters. Although τ_o may not be exactly constant when N is varied, we have achieved a reasonable description of all simulation data for both ring and linear polymers having variable N based on the above procedure, as shown in Fig. 5(c). Nevertheless, it should be emphasized again that the fitted results may still have factors that contribute to uncertainties.

To illustrate the dependence of τ_α on N more explicitly, Fig. 6 shows τ_α as a function of N for a range of T for both ring and linear polymer melts. At high T, τ_α for both ring and linear polymer melts exhibit little variation with N. This is true even at low T for ring polymer melts. However, as temperature decreases, τ_α for linear polymer melts first increases with increasing N and then tends to plateau at large N, a trend that is consistent with measurements.

Characteristic Temperatures and Fragility of Glass Formation

The glass formation is a broad thermodynamic transition with multiple characteristic temperatures rather than a conventional phase transition. This aspect has been emphasized by the GET,[64–67] which is capable of capturing the essential trends in the characteristic temperatures of glass formation. These characteristic temperatures include the onset at T_A, the middle or crossover at T_c, and the termination at T_0 of glass formation, as well as the common glass transition temperature T_g, where T_0 is often referred to as the "ideal glass transition temperature", as mentioned earlier. Below, we determine the characteristic

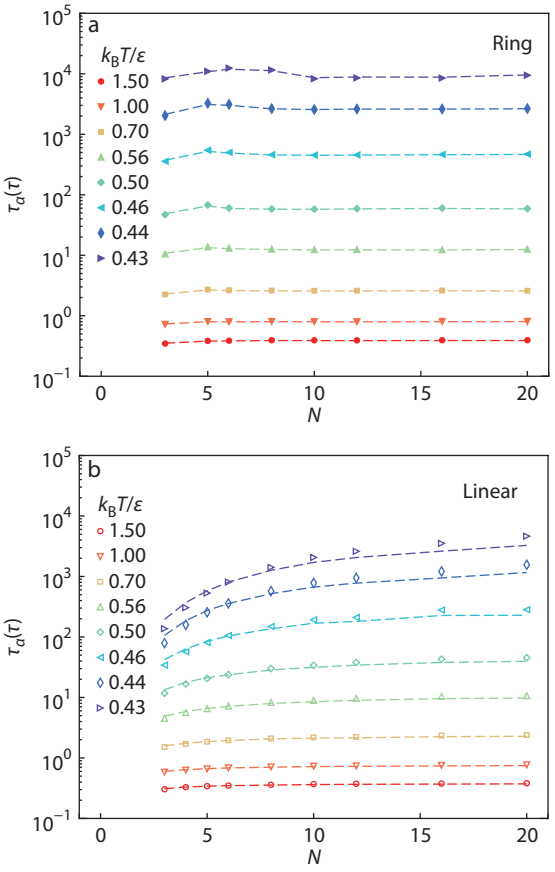

Fig. 6 τ_α as a function of N for a range of T. Panels (a) and (b) correspond to the results for ring and linear polymer melts, respectively. Lines are a guide to the eye.

https://doi.org/10.1007/s10118-023-3004-5

temperatures and fragility of polymer glass formation based on our simulation data using the method established in our previous works,[86–92] which we briefly describe below.

The onset temperature T_A is determined on the basis of the mean squared displacement (MSD),[103–105]

$$\left\langle r^2(t) = \frac{1}{N_b}\sum_{j=1}^{N_b}\left|r_j(t) - r_j(t_0)\right|^2\right\rangle \quad (9)$$

More specifically, the onset temperature is identified by the appearance of a minimum around t=1 τ in the logarithmic derivative of the MSD, $\partial \ln r^2(t)/\partial \ln(t)$. The timescale defining T_A is closely related to the particle localization,[106,107] and hence, T_A is also referred to as the localization temperature. Above T_A, a high-temperature Arrhenius regime typically exists in the dynamics of glass-forming liquids, as discussed earlier.

The crossover temperature T_c is determined by fitting simulation data with 5 $\tau < \tau_\alpha < 5\times10^3$ τ for each N to a power-law equation, $\tau_\alpha \sim (T - T_c)^{-\gamma}$, where γ is a fitting parameter. This power-law scaling has been widely discussed within the mode-coupling theory framework,[108] and the fitted critical temperature T_c is often termed the "mode-coupling temperature". The GET also predicts that the power-law form applies to τ_α over a limited T range above T_c but below the onset temperature, T_A,[64] where T_c can be precisely defined based on a thermodynamic condition and this characteristic temperature separates the dynamics of the glass-forming liquids into two distinct regimes. It should be noted that the power-law relation is only used in the present work to determine the general trend of T_c as a function of N, and no further analysis is conducted in relation to the mode-coupling theory.

Finally, T_0 and T_g are determined from the VFT fits to the simulation data, as described above. This approach provides a reasonable description of all our simulation data and yields relatively reliable estimates of T_0. We then estimate T_g by approximating 1 reduced time unit as 1 ps and by using the common empirical definition of T_g, *i.e.*, $\tau_\alpha(T_g) = 100$ s. Alternatively, T_g can be estimated from the T dependence of the density or specific volume during a cooling process, where a kink is typically utilized to define the temperature at where the glass transition occurs. This method should yield estimates of T_g that are qualitatively similar to those based on the VFT fits, although some quantitative differences might be expected between the two methods. It should be emphasized that our estimates of T_g are only utilized to indicate the qualitative trends in polymer glass formation in the present work. All simulation estimates of T_g are subject to significant uncertainties, and the approach in the present work has the virtue of simplicity.

Despite extensive studies on the mass dependence of glass formation in ring polymers, a clear conclusion has not been reached yet. Our simulation data allow us to perform a more detailed analysis of the characteristic temperatures T_x ($x = A$, c, g, or 0) of glass formation in ring and linear polymer melts. These results are summarized in Fig. 7. For linear polymer melts, our simulation results indicate that T_x increases with increasing N and gradually approaches a plateau at large N. We further find that the relationship between T_x and N can be well described by the empirical Flory-Fox equation,[109]

$$T_x = T_{x,\infty} - \frac{K_x}{N} \quad (10)$$

where $T_{x,\infty}$ and K_x are fitting parameters. Turning to the results for ring polymer melts, the characteristic temperatures remain nearly unchanged as N is varied. Our simulation results also indicate that T_x for ring polymers is generally higher than that for linear polymers at the same N. However, the difference between the T_x of ring and linear polymers become progressively diminished as N increases, consistent with existing experimental results.[2,40,46,47,50–55,58,59,61,62] These findings indicate that the influence of chain topology on polymer glass formation weakens as N increases, as expected.

It should be pointed out that although the mass dependence of T_g has been found to be generally weaker in ring polymers than in linear polymers in experiment, T_g still varies with N to some extent in the low molecular mass regime.[55–59] This is in contrast to the present simulation results showing nearly no dependence of T_g on molecular mass. This evidently points to the fact that the present coarse-grained polymer model is inadequate to fully capture the mass dependence of glass formation in ring polymers. Even in the case of linear polymer melts, we emphasize that the mass dependence of T_g in our polymer model is much weaker than that in real polymers. For instance, T_g can be varied by a factor of 1.2–1.6 by changing the molecular mass over a large change in experiment.[110,111] By contrast, our simulation results indicate that T_g is increased by a factor less than 1.1 when N is increased from 3 to 20, as shown in Fig. 7(c). We expect that the inclusion of higher-order intramolecular potentials, such as angle and torsional potentials, should be highly important for quantitatively recovering trends observed in the mass dependence of glass formation of real polymers. Our coarse-grained polymer model is rather idealized, so future work is required to assess the individual importance of additional interactions.

Regarding the dependence of fragility of glass formation on molecular mass, Fig. 8 displays the ratio T_0/T_A as a function of N for both ring and linear polymer melts. Calculations based on the GET indicate that there is unique correspondence between D and T_0/T_A in polymer melts with a broad range of chain stiffness and cohesive energy parameters,[112,113] so the overall breadth of glass formation provides an alternative measure of fragility. As discussed above, the VFT fragility index D is highly sensitive to the range of T for the fittings, and previous studies have noted the difficulty of estimating the fragility index using the VFT equation to fit the data over a T regime much higher than T_g.[86,88] In the present study, we obtained meaningful fitting results for T_0, but a reliable trend for D cannot be determined, a situation that also occurs in polymer melts having variable cohesive interaction strength considered in our previous work.[88] In contrast to D, T_0 is relatively insensitive to the fitting procedure, and hence, the fragility characterized by T_0/T_A should be more reliable.

As shown in Fig. 8, the fragility of linear polymer melts increases with increasing N and tends to plateau at large N. By contrast, the fragility of ring polymer melts is nearly independent of N. These trends are basically the same as that found for T_x. Quantitively, the fragility of ring polymers is higher than that of linear polymers. Therefore, we can conclude from our simulations that the characteristic temperat-

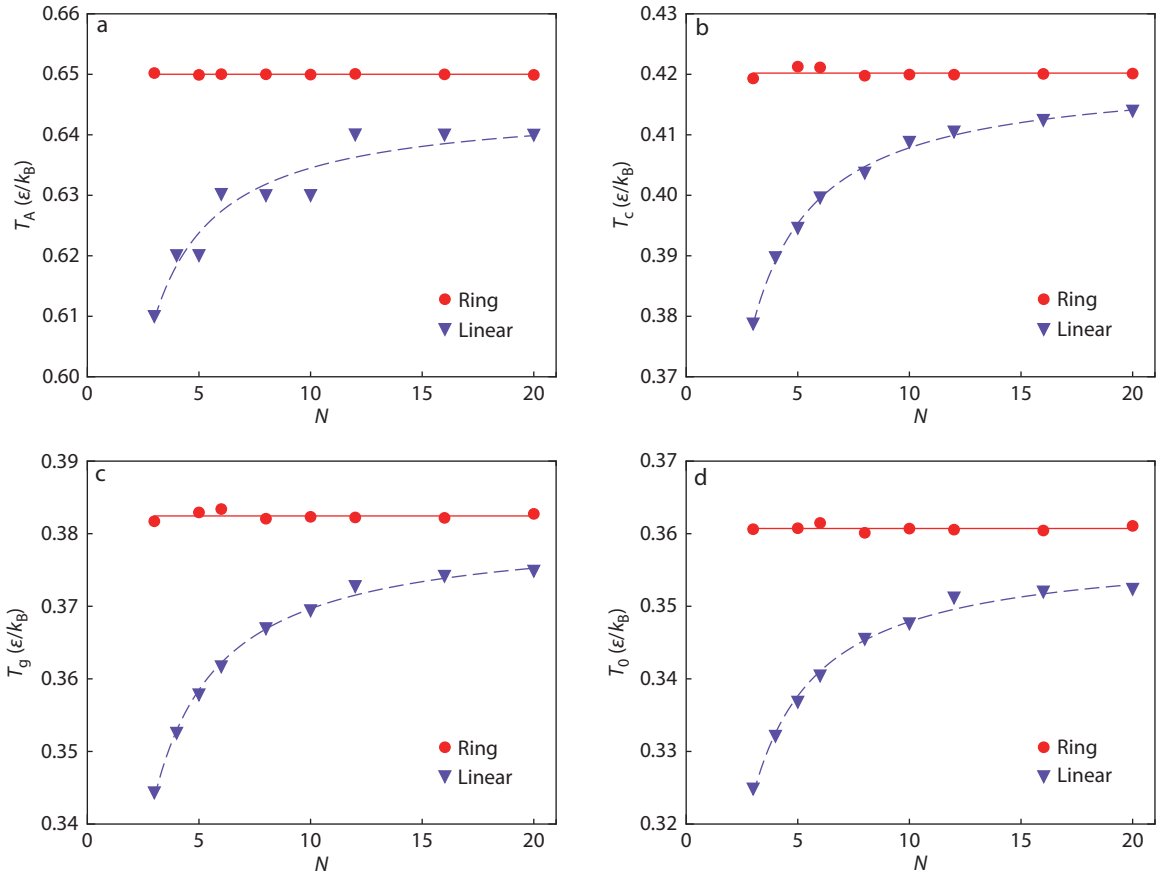

Fig. 7 Characteristic temperatures T_x (x = A, c, g, or 0) of glass formation as a function of N for ring and linear polymer melts. Panels (a–d) correspond to the results for the onset temperature T_A, crossover temperature T_c, glass transition temperature T_g, and ideal glass transition temperature T_0, respectively. Dashed lines indicate the fits of simulation data to Eq. (10) for linear polymer melts. Solid lines are a guide to the eye for ring polymer melts.

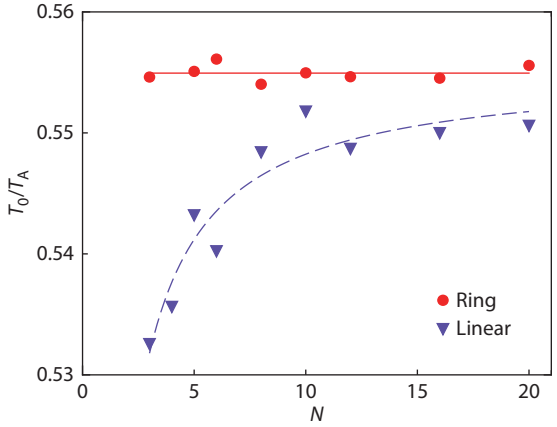

Fig. 8 Fragility of glass formation as a function of N for ring and linear polymer melts, characterized by the overall breadth of glass formation, T_0/T_A. Lines are a guide to the eye.

ures and fragility of glass formation increase with increasing molecular mass in linear polymers, but the mass dependences of these properties are rather weak in the family of ring polymer models considered. These general trends are broadly consistent with experimental measurements.[2,40,46,47,50–52,55,58,59,61–63]

String Model Description of Glass Formation

In this section, we utilize the string model to gain insight into the mass dependence of glass formation in our polymer model. The GET framework has been under active development,[64–67] which offers a promising theory for understanding the thermodynamics and dynamics of glass-forming polymers. As mentioned earlier, the GET combines the LCT[68,69] for the thermodynamics of polymer systems having explicit monomer structures and architectures with the AG postulated relation[70] between the structural relaxation time and the configurational entropy. However, computing the configurational entropy is a challenging task for polymer systems based on MD simulations.[94] Therefore, we focus on the string model of glass formation in the present work,[65,74,75] which is broadly consistent with the GET but uses quantities that are more easily accessible from MD simulations.

Extensive simulations[74,91,92,95,98,99,103–105,114–117] revealed that the most mobile particles in glass-forming liquids form string-like structures, which are defined in terms of their cooperative exchange motion over the lifetime in which the strings exist. This cooperative motion aligns with the philosophical assumptions of the AG model[70] and provides a quantitative realization of the hypothetical CRR proposed by AG.[70] However, the AG theory does not offer a quantitative picture of the structure and polydispersity of the CRR. De-

https://doi.org/10.1007/s10118-023-3004-5

tailed studies demonstrated that the size of string-like clusters indeed provides the most consistent form of dynamic heterogeneity in relation to the properties of the CRR. The validity of the string model has been confirmed in a wide range of polymeric and other GF materials.[74,91,92,95,98,99,103–105,114–117] Moreover, the model is further supported by a theoretical analysis by Freed.[75] We recently provided comprehensive reviews on the GET and string model approaches to glass formation,[65–67] and the reader is referred to these reviews for a detailed discussion of the string model.[65]

We employ the established procedure to quantify the string-like cooperative motion in our simulations.[118] We define the most mobile particles as the f_0=6.5% of particles with the greatest displacement over any chosen interval. This fraction was chosen based on the following considerations. In previous works,[94,119] it has been found that the mobile particles typically account for 5%–7% of the total particles. Hence, we use 6.5% as a reasonable choice, in accord with previous studies on the glass formation of polymer systems.[89,91,93,120] Starr *et al.*[94] suggested a general methodology for estimating this fraction for any given fluid, and the reader is referred to this work for a detailed discussion. Subsequently, the mobile particles are decomposed into subsets of string-like groups of cooperatively moving particles. Specifically, two mobile particles j and k are then considered to be in the same string if the following condition holds,

$$\min\left[\left|\mathbf{r}_j(t)-\mathbf{r}_k(0)\right|,\left|\mathbf{r}_k(t)-\mathbf{r}_j(0)\right|\right]<\delta \tag{11}$$

where δ is a displacement distance parameter that we set to be 0.55 σ. This value is consistent with that used in previous simulations of various polymer systems.[86,88,91,92] The number-averaged string length $\langle s(t)\rangle$ is then calculated *via* $\langle s(t)\rangle = \langle\sum_{s=1}^{\infty} s\cdot C(s)\rangle/\sum_{s=1}^{\infty} C(s)$, with $C(s)$ being the probability of finding a string of length s. As an illustration, Fig. 9(a) exhibits $\langle s(t)\rangle$ as a function of t at different T for both ring and linear polymers with N=20. It is observed that $\langle s(t)\rangle$ displays a maximum $L \equiv \langle s(t_L)\rangle$ at a characteristic time t_L, where L defines the characteristic string length and t_L is the corresponding characteristic "lifetime" of strings. A typical configuration of strings at the time where $\langle s(t)\rangle$ is maximal is illustrated in Fig. 9(b) for the ring polymer melt with N=20 at k_BT/ε=0.43.

Fig. 10 summarizes and compares the variation of L with N

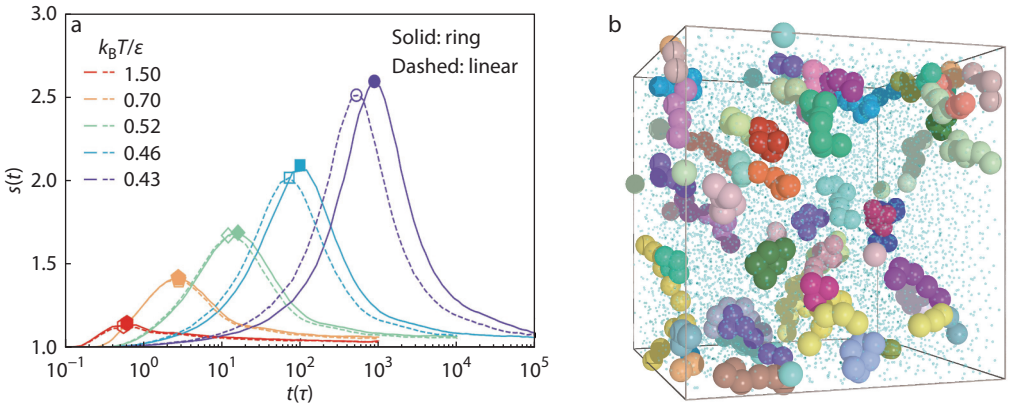

Fig. 9 (a) Number-averaged string length $\langle s(t)\rangle$ as a function of t at varying T for ring and linear polymer melts with N = 20. Solid and dashed lines correspond to the results for ring and linear polymer melts, respectively. (b) A typical configuration of strings at the time where $\langle s(t)\rangle$ is maximal for the ring polymer melt with N = 20 at k_BT/ε = 0.43. Each string is represented by large spheres in a different color, and the other polymer segments are depicted as small dots. Only strings with a length greater than 3 are shown for clarity purposes.

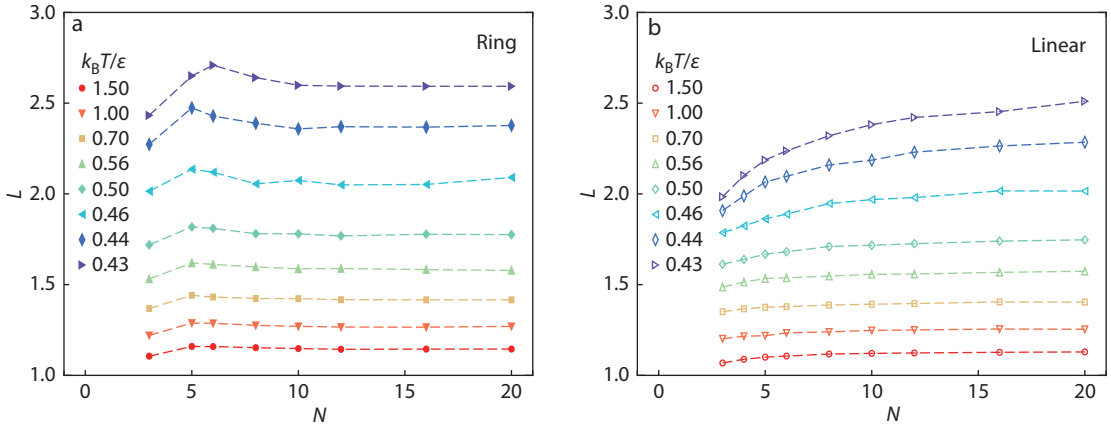

Fig. 10 Average string length L as a function of N for a range of T. Panels (a) and (b) correspond to the results for ring and linear polymer melts, respectively. Lines are a guide to the eye.

https://doi.org/10.1007/s10118-023-3004-5

over a wide range of T for ring and linear polymers. As can be seen, L increases modestly with N at low T in linear polymer melts, whereas it seems that L exhibits a more complicated dependence on N in ring polymer melts, particularly at low T. The non-monotonic variation of L with N is likely related to the structural features discussed earlier that arise from topological constraints in small rings.

To describe the non-Arrhenius dynamics at temperatures below T_A, the activation free energy ΔG for structural relaxation is assumed by the string model to be proportional to the average string length L normalized by its value at the onset temperature T_A.[65,74,75] This essentially leads to a temperature-dependent activation free energy given by $\Delta G(T) = G_o(L/L_A)$, where L_A is the value of L at T_A. The structural relaxation time then takes the following form,

$$\tau_\alpha = \tau_o \exp\left(\frac{\Delta G_o}{k_B T}\frac{L}{L_A}\right) \quad (12)$$

To reduce the number of adjustable parameters, the parameter τ_o can be eliminated from the knowledge of τ_α at T_A,[104] resulting in the following equation:

$$\tau_\alpha = \tau_\alpha(T_A)\exp\left(\frac{\Delta H_o - T\Delta S_o}{k_B T}\frac{L}{L_A} - \frac{\Delta H_o - T_A\Delta S_o}{k_B T_A}\right) \quad (13)$$

where ΔH_o is determined from the Arrhenius equation in the high T regime, as discussed earlier. Therefore, ΔS_o is the only remaining free fitting parameter, which is notoriously difficult to treat theoretically and is the primary source of uncertainty in TST. Theoretical estimation of ΔS_o presents a significant challenge in the GET, as discussed in Refs. [65,110,111,121]. We find that all our simulation data for both ring and linear polymer melts can be described satisfactorily by the string model of glass formation, as shown in Fig. 11.

The string model also allows us to investigate how chain length and topology affect the energetic parameters, ΔH_o and ΔS_o. Fig. 12 shows ΔH_o and ΔS_o as a function N. In linear polymer melts, ΔH_o increases as N increases and gradually reaches a plateau, while ΔS_o shows an opposite trend. Hence, these two parameters exhibit a correlation that is akin to the entropy-enthalpy compensation (EEC) effect.[122] In contrast,

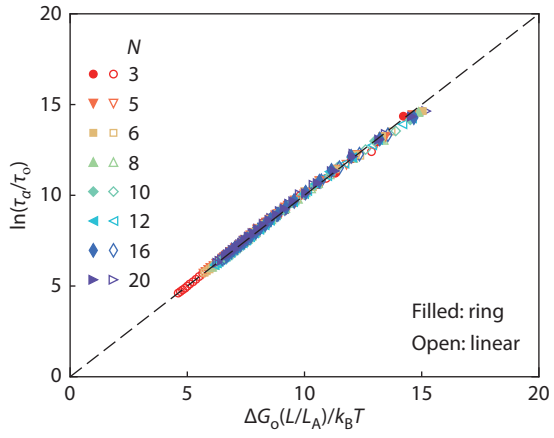

Fig. 11 String model description of the relationship between τ_α and L for polymer melts having variable N. Filled and open symbols correspond to the results for ring and linear polymer melts, respectively. The dashed line indicates $\ln(\tau_\alpha/\tau_o) = \Delta G_o(L/L_A)/k_BT$.

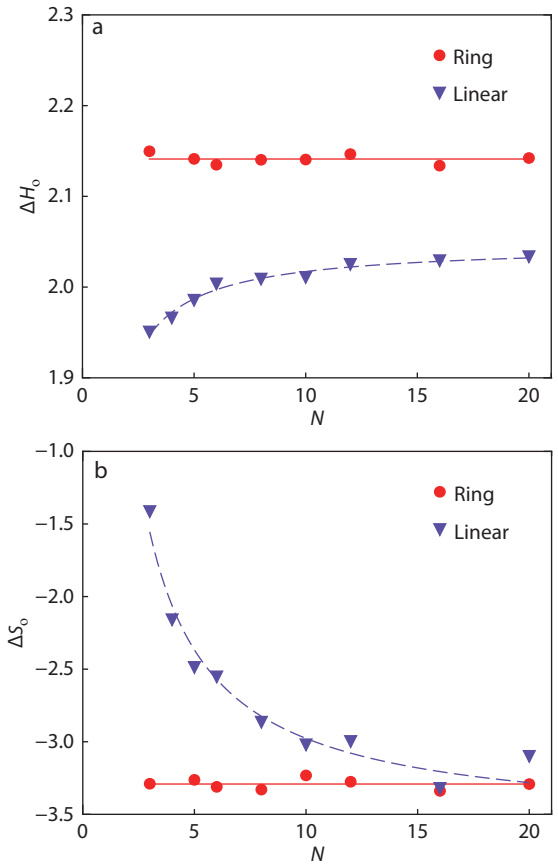

Fig. 12 (a) Enthalpy ΔH_o and (b) entropy ΔS_o of high-T activation as a function of N for ring and linear polymer melts. Lines are a guide to the eye.

both ΔH_o and ΔS_o remain nearly unchanged in ring polymer melts. Notably, the absolute magnitude of ΔS_o becomes larger with increasing N in linear polymers, implying that the entropic contribution to the activation free energy, which is neglected in the AG theory[70] and the GET,[64,65] becomes more important at larger N. This observation, along with our previous findings,[86–88,92] emphasizes the role of the activation entropy in achieving the quantitative description and prediction of polymer glass formation, which is currently a major challenge in the GET.[65] We also note that ΔS_o is generally negative in our polymer models, a phenomenon observed in many GF systems,[86–88,104] including ion-containing[91] and graft[92] polymers, although this phenomenon has not been fully understood.

Our simulation results imply that the configurational entropy-based theories provide a promising framework for understanding the glass formation of ring polymers, even though small ring polymers exhibit strong interchain correlations that are normally absent in linear polymers and large ring polymers. It is then highly desirable to incorporate the cyclic topology into the existing frameworks, such as the LCT.[68,69]

CONCLUSIONS

In summary, extensive molecular dynamics simulations were

performed to investigate the phenomenology of the structural and dynamic properties of unknotted, nonconcatenated ring polymers having variable molecular mass upon approaching the glass transition temperature. The glass formation of ring polymer melts has been compared and contrasted with that of linear polymer melts, allowing us to discern the features induced by the cyclic topology in the mass dependence of polymer glass formation. We identified an unusual property associated with the occurrence of a characteristic peak in the static structure factor of small ring polymers, and a detailed analysis indicates that this feature arises from the strong interchain correlations and disappears in the large molecular mass limit. The mass dependence of the structural relaxation time over a wide range of temperatures were examined in both ring and linear polymers. Consistent with experimental observations, the characteristic temperatures and fragility of glass formation increase with increasing molecular mass in linear polymer melts, while the mass dependences of these properties are rather weak in the ring polymer models considered. The difference between the characteristic properties of glass formation of ring and linear polymers becomes larger at lower molecular masses, and the glass transition temperature of ring polymers is generally higher than that of linear polymers at the same molecular mass. Moreover, the asymptotic values of the glass transition temperature tend to be the same for both ring and linear polymer melts, which is again consistent with existing experimental results. Finally, we showed that the glass formation of both ring and linear polymer melts can be quantitatively described by the string model, which can be regarded as a configurational-based model that takes the mass of string-like clusters as a molecular realization of the abstract cooperatively rearranging regions, as envisioned by Adam and Gibbs.[70] This finding opens the possibility of applying the generalized entropy theory to describe the glass formation of ring polymers by incorporating the ring topology into the theoretical framework. Overall, our work provides firm observational data for facilitating the development of theories of glass formation of ring polymers.

Conflict of Interests

The authors declare no interest conflict.

ACKNOWLEDGMENTS

This work was financially supported by the National Natural Science Foundation of China (Nos. 22222307 and 21973089).

REFERENCES

1 Hadziioannou, G.; Cotts, P. M.; ten Brinke, G.; Han, C. C.; Lutz, P.; Strazielle, C.; Rempp, P.; Kovacs, A. J. Thermodynamic and hydrodynamic properties of dilute solutions of cyclic and linear polystyrenes. *Macromolecules* **1987**, *20*, 493–497.
2 Alberty, K. A.; Hogen-Esch, T. E.; Carlotti, S. Synthesis and characterization of macrocyclic vinyl-aromatic polymers. *Macromol. Chem. Phys.* **2005**, *206*, 1035–1042.
3 Lonsdale, D. E.; Monteiro, M. J. Various polystyrene topologies built from tailored cyclic polystyrene *via* CuAAC reactions. *Chem. Commun.* **2010**, *46*, 7945–7947.
4 Zimm, B. H.; Stockmayer, W. H. The dimensions of chain molecules containing branches and rings. *J. Chem. Phys.* **1949**, *17*, 1301–1314.
5 Kramers, H. A. The behavior of macromolecules in inhomogeneous flow. *J. Chem. Phys.* **1946**, *14*, 415–424.
6 Roovers, J. Viscoelastic properties of polybutadiene rings. *Macromolecules* **1988**, *21*, 1517–1521.
7 Pasquino, R.; Vasilakopoulos, T. C.; Jeong, Y. C.; Lee, H.; Rogers, S.; Sakellariou, G.; Allgaier, J.; Takano, A.; Brás, A. R.; Chang, T.; Gooßen, S.; Pyckhout-Hintzen, W.; Wischnewski, A.; Hadjichristidis, N.; Richter, D.; Rubinstein, M.; Vlassopoulos, D. Viscosity of ring polymer melts. *ACS Macro Lett.* **2013**, *2*, 874–878.
8 Jeong, Y.; Jin, Y.; Chang, T.; Uhlik, F.; Roovers, J. Intrinsic viscosity of cyclic polystyrene. *Macromolecules* **2017**, *50*, 7770–7776.
9 Kapnistos, M.; Lang, M.; Vlassopoulos, D.; Pyckhout-Hintzen, W.; Richter, D.; Cho, D.; Chang, T.; Rubinstein, M. Unexpected power-law stress relaxation of entangled ring polymers. *Nat. Mater.* **2008**, *7*, 997–1002.
10 Vargas–Lara, F.; Hassan, A. M.; Mansfield, M. L.; Douglas, J. F. Knot energy, complexity, and mobility of knotted polymers. *Sci. Rep.* **2017**, *7*, 13374.
11 Vargas-Lara, F.; Pazmiño Betancourt, B. A.; Douglas, J. F. Communication: a comparison between the solution properties of knotted ring and star polymers. *J. Chem. Phys.* **2018**, *149*, 161101.
12 Morgese, G.; Trachsel, L.; Romio, M.; Divandari, M.; Ramakrishna, S. N.; Benetti, E. M. Topological polymer chemistry enters surface science: linear versus cyclic polymer brushes. *Angew. Chem. Int. Ed.* **2016**, *55*, 15583–15588.
13 Liénard, R.; De Winter, J.; Coulembier, O. Cyclic polymers: Advances in their synthesis, properties, and biomedical applications. *J. Polym. Sci.* **2020**, *58*, 1481–1502.
14 Romio, M.; Trachsel, L.; Morgese, G.; Ramakrishna, S. N.; Spencer, N. D.; Benetti, E. M. Topological polymer chemistry enters materials science: expanding the applicability of cyclic polymers. *ACS Macro Lett.* **2020**, *9*, 1024–1033.
15 Cai, X.; Liang, C.; Liu, H.; Zhang, G. Conformation and structure of ring polymers in semidilute solutions: a molecular dynamics simulation study. *Polymer* **2022**, *253*, 124953.
16 Cai, X.; Liu, H.; Zhang, G. Control of the threading ratio of rings in a polypseudorotaxane: a computer simulation study. *Polymer* **2023**, *268*, 125705.
17 Chen, Y. X.; Cai, X. Q.; Zhang, G. J. Topological catenation enhances elastic modulus of single linear polycatenane. *Chinese J. Polym. Sci.* **2023**, *41*, DOI: 10.1007/s10118-023-2902-x.
18 Lei, H.; Zhang, J.; Wang, L.; Zhang, G. Dimensional and shape properties of a single linear polycatenane: effect of catenation topology. *Polymer* **2021**, *212*, 123160.
19 Kruteva, M.; Allgaier, J.; Monkenbusch, M.; Hoffmann, I.; Richter, D. Structure and dynamics of large ring polymers. *J. Rheol.* **2021**, *65*, 713–727.
20 Wu, Z. T.; Zhou, J. J. Mechanical properties of interlocked-ring polymers: a molecular dynamics simulation study. *Chinese J. Polym. Sci.* **2019**, *37*, 1298–1304.
21 Halverson, J. D.; Lee, W. B.; Grest, G. S.; Grosberg, A. Y.; Kremer, K. Molecular dynamics simulation study of nonconcatenated ring polymers in a melt. I. Statics. *J. Chem. Phys.* **2011**, *134*, 204904.
22 Halverson, J. D.; Lee, W. B.; Grest, G. S.; Grosberg, A. Y.; Kremer, K. Molecular dynamics simulation study of nonconcatenated ring polymers in a melt. II. Dynamics. *J. Chem. Phys.* **2011**, *134*, 204905.
23 Wang, L.; Xu, L.; Liu, B.; Shi, T.; Jiang, S.; An, L. The influence of polymer architectures on the dewetting behavior of thin

polymer films: from linear chains to ring chains. *Soft Matter* **2017**, *13*, 3091–3098.
24 Zhu, L.; Li, J.; Li, H.; Liu, B.; Chen, J.; Jiang, S. The role of entanglement in crystallization and melting of cyclic poly(ε-caprolactone)s. *CrystEngComm* **2023**, *25*, 1383–1392.
25 Zhang, H.; Lv, T.; Li, J.; Liu, B.; Jiang, S. Pendant affected crystallization behaviors of cyclic poly(ε-caprolactone). *Crystal Growth & Design* **2019**, *19*, 49–54.
26 Semlyen, J. A. *Cyclic polymers*. 2nd ed.; Kluwer Academic: Dordrecht: The Netherlands, **2000**, p. 790.
27 Ree, B. J.; Satoh, T.; Yamamoto, T. Micelle structure details and stabilities of cyclic block copolymer amphiphile and its linear analogues. *Polymers* **2019**, *11*, 163.
28 Wang, C. E.; Wei, H.; Tan, N.; Boydston, A. J.; Pun, S. H. Sunflower polymers for folate-mediated drug delivery. *Biomacromolecules* **2016**, *17*, 69–75.
29 Tu, X. Y.; Meng, C.; Wang, Y. F.; Ma, L. W.; Wang, B.-Y.; He, J. L.; Ni, P. H.; Ji, X. L.; Liu, M. Z.; Wei, H. Fabrication of thermosensitive cyclic brush copolymer with enhanced therapeutic efficacy for anticancer drug delivery. *Macromol. Rapid Commun.* **2018**, *39*, 1700744.
30 Wei, H.; Chu, D. S. H.; Zhao, J.; Pahang, J. A.; Pun, S. H. Synthesis and evaluation of cyclic cationic polymers for nucleic acid delivery. *ACS Macro Lett.* **2013**, *2*, 1047–1050.
31 Fu, C.; Lin, L.; Shi, H.; Zheng, D.; Wang, W.; Gao, S.; Zhao, Y.; Tian, H.; Zhu, X.; Chen, X. Hydrophobic poly(amino acid) modified PEI mediated delivery of rev-casp-3 for cancer therapy. *Biomaterials* **2012**, *33*, 4589–4596.
32 Wang, J.; Lei, Y.; Xie, C.; Lu, W.; Yan, Z.; Gao, J.; Xie, Z.; Zhang, X.; Liu, M. Targeted gene delivery to glioblastoma using a C-end rule RGERPPR peptide-functionalised polyethylenimine complex. *Int. J. Pharm.* **2013**, *458*, 48–56.
33 Golba, B.; Benetti, E. M.; De Geest, B. G. Biomaterials applications of cyclic polymers. *Biomaterials* **2021**, *267*, 120468.
34 Ball, M.; Zhong, Y.; Fowler, B.; Zhang, B.; Li, P.; Etkin, G.; Paley, D. W.; Decatur, J.; Dalsania, A. K.; Li, H. Macrocyclization in the design of organic n-type electronic materials. *J. Am. Chem. Soc.* **2016**, *138*, 12861–12867.
35 Miao, Z.; Esper, A. M.; Nadif, S. S.; Gonsales, S. A.; Sumerlin, B. S.; Veige, A. S. Semi-conducting cyclic copolymers of acetylene and propyne. *React. Funct. Polym.* **2021**, *169*, 105088.
36 Singh, M.; Dong, M.; Wu, W.; Nejat, R.; Tran, D. K.; Pradhan, N.; Raghavan, D.; Douglas, J. F.; Wooley, K. L.; Karim, A. Enhanced dielectric strength and capacitive energy density of cyclic polystyrene films. *ACS Polym. Au* **2022**, *2*, 324–332.
37 Freifelder, D.; Kleinschmidt, A. K.; Sinsheimer, R. L. Electron microscopy of single-stranded DNA: circularity of DNA ofbacteriophage φX174. *Science* **1964**, *146*, 254–255.
38 Wasserman, S. A.; Cozzarelli, N. R. Biochemical topology: applications to DNA recombination and replication. *Science* **1986**, *232*, 951–960.
39 Saether, O.; Craik, D. J.; Campbell, I. D.; Sletten, K.; Juul, J.; Norman, D. G. Elucidation of the primary and three-dimensional structure of the uterotonic polypeptide Kalata B1. *Biochemistry* **1995**, *34*, 4147–4158.
40 Haque, F. M.; Grayson, S. M. The synthesis, properties and potential applications of cyclic polymers. *Nat. Chem.* **2020**, *12*, 433–444.
41 Jr., T. G. F.; Flory, P. J. Second-order transition temperatures and related properties of polystyrene. I. Influence of molecular weight. *J. Appl. Phys.* **1950**, *21*, 581–591.
42 Fox, T. G.; Flory, P. J. The glass temperature and related properties of polystyrene. Influence of molecular weight. *J. Polym. Sci.* **1954**, *14*, 315–319.
43 Tito, N. B.; Lipson, J. E. G.; Milner, S. T. Lattice model of dynamic heterogeneity and kinetic arrest in glass-forming liquids. *Soft Matter* **2013**, *9*, 3173–3180.
44 White, R. P.; Lipson, J. E. G. Polymer free volume and its connection to the glass transition. *Macromolecules* **2016**, *49*, 3987–4007.
45 Rique-Lurbet, L.; Schappacher, M.; Deffieux, A. A new strategy for the synthesis of cyclic polystyrenes: principle and application. *Macromolecules* **1994**, *27*, 6318–6324.
46 Zhang, L.; Elupula, R.; Grayson, S. M.; Torkelson, J. M. Suppression of the fragility-confinement effect *via* low molecular weight cyclic or ring polymer topology. *Macromolecules* **2017**, *50*, 1147–1154.
47 Gao, L.; Oh, J.; Tu, Y.; Chang, T.; Li, C. Y. Glass transition temperature of cyclic polystyrene and the linear counterpart contamination effect. *Polymer* **2019**, *170*, 198–203.
48 Schappacher, M.; Deffieux, A. Synthesis of macrocyclic poly(2-chloroethyl vinyl ether)s. *Makromol. Chem., Rapid Commun.* **1991**, *12*, 447–453.
49 Deffieux, A.; Schappacher, M.; Rique-Lurbet, L. New routes to macrocyclic polymers of controlled dimensions. *Polymer* **1994**, *35*, 4562–4568.
50 Kammiyada, H.; Ouchi, M.; Sawamoto, M. A study on physical properties of cyclic poly(vinyl ether)s synthesized *via* ring-expansion cationic polymerization. *Macromolecules* **2017**, *50*, 841–848.
51 Xu, X.; Zhou, N.; Zhu, J.; Tu, Y.; Zhang, Z.; Cheng, Z.; Zhu, X. The first example of main-chain cyclic azobenzene polymers. *Macromol. Rapid Commun.* **2010**, *31*, 1791–1797.
52 Pipertzis, A.; Hossain, M. D.; Monteiro, M. J.; Floudas, G. Segmental dynamics in multicyclic polystyrenes. *Macromolecules* **2018**, *51*, 1488–1497.
53 Gan, Y.; Dong, D.; Hogen-Esch, T. E. Effects of lithium bromide on the glass transition temperatures of linear and macrocyclic poly(2-vinylpyridine) and polystyrene. *Macromolecules* **1995**, *28*, 383–385.
54 Nossarev, G. G.; Hogen-Esch, T. E. Synthesis and thermal properties of macrocyclic poly(2-vinylnaphthalene) containing single 1,4-benzylidene or 9,10-anthracenylidene groups. *Macromolecules* **2002**, *35*, 1604–1610.
55 Clarson, S. J.; Dodgson, K.; Semlyen, J. A. Studies of cyclic and linear poly(dimethylsiloxanes): 19. Glass-transition temperatures and crystallization behavior. *Polymer* **1985**, *26*, 930–934.
56 Baljon, A. R. C.; Mendoza, G.; Balabaev, N. K.; Lyulin, A. V. Glass-transition temperature of cyclic polystyrene: a computational study. *Polym. Sci. Ser. A* **2021**, *63*, 356–362.
57 Chremos, A.; Douglas, J. F. Communication: when does a branched polymer become a particle. *J. Chem. Phys.* **2015**, *143*, 111104.
58 Hogen-Esch, T. E.; Sundararajan, J.; Toreki, W. Synthesis and characterization of topologically interesting vinyl polymers. *Makromol. Chem., Macromol. Symp.* **1991**, *47*, 23–42.
59 Yang, A. J. M.; Di Marzio, E. A. Glass temperature of polymer ring systems. *Macromolecules* **1991**, *24*, 6012–6018.
60 Di Marzio, E. A.; Guttman, C. M. The glass temperature of polymer rings. *Macromolecules* **1987**, *20*, 1403–1407.
61 Clarson, S. J.; Semlyen, J. A.; Dodgson, K. Cyclic polysiloxanes: 4. Glass transition temperatures of poly(phenylmethylsiloxanes). *Polymer* **1991**, *32*, 2823–2827.
62 Liu, X.; Chen, D.; He, Z.; Zhang, H.; Hu, H. Molecular weight dependence of the glass transition of cyclic polystyrene. *Polym. Commun.* **1991**, *32*, 123–125.
63 Kirst, K. U.; Kremer, F.; Pakula, T.; Hollingshurst, J. Molecular dynamics of cyclic and linear poly(dimethylsiloxanes). *Colloid. Polym. Sci.* **1994**, *272*, 1420–1429.

https://doi.org/10.1007/s10118-023-3004-5

64 Dudowicz, J.; Freed, K. F.; Douglas, J. F. Generalized entropy theory of polymer glass formation. *Adv. Chem. Phys.* **2008**, *137*, 125–222.
65 Xu, W. S.; Douglas, J. F.; Sun, Z. Y. Polymer glass formation: role of activation free energy, configurational entropy, and collective motion. *Macromolecules* **2021**, *54*, 3001–3033.
66 Xu, W. S.; Sun, Z. Y. A thermodynamic perspective on polymer glass formation. *Chinese J. Polym. Sci.* **2023**, 10.1007/s10118-023-2896-4.
67 Yuan, Q. L.; Yang, Z.; Xu, W. S. Advances in the generalized entropy theory of polymer glass formation. *Sci. Sin.: Chim.* **2023**, *53*, 616–627.
68 Foreman, K. W.; Freed, K. F. Lattice cluster theory of multicomponent polymer systems: chain semiflexibility and specific interactions. *Adv. Chem. Phys.* **1998**, *103*, 335–390.
69 Xu, W.-S.; Freed, K. F. Lattice cluster theory for polymer melts with specific interactions. *J. Chem. Phys.* **2014**, *141*, 044909.
70 Adam, G.; Gibbs, J. H. On the temperature dependence of cooperative relaxation properties in glass-forming liquids. *J. Chem. Phys.* **1965**, *43*, 139–146.
71 Vargas-Lara, F.; Pazmiño Betancourt, B. A.; Douglas, J. F. Influence of knot complexity on glass-formation in low molecular mass ring polymer melts. *J. Chem. Phys.* **2019**, *150*, 101103.
72 Braghetto, A.; Kundu, S.; Baiesi, M.; Orlandini, E. Machine learning understands knotted polymers. *Macromolecules* **2023**, *56*, 2899–2909.
73 Santangelo, P. G.; Roland, C. M.; Chang, T.; Cho, D.; Roovers, J. Dynamics near the glass temperature of low molecular weight cyclic polystyrene. *Macromolecules* **2001**, *34*, 9002–9005.
74 Pazmiño Betancourt, B. A.; Douglas, J. F.; Starr, F. W. String model for the dynamics of glass-forming liquids. *J. Chem. Phys.* **2014**, *140*, 204509.
75 Freed, K. F. Communication: towards first principles theory of relaxation in supercooled liquids formulated in terms of cooperative motion. *J. Chem. Phys.* **2014**, *141*, 141102.
76 Kremer, K.; Grest, G. S. Dynamics of entangled linear polymer melts: a molecular-dynamics simulation. *J. Chem. Phys.* **1990**, *92*, 5057–5086.
77 Grest, G. S.; Kremer, K. Molecular dynamics simulation for polymers in the presence of a heat bath. *Phys. Rev. A* **1986**, *33*, 3628–3631.
78 Weeks, J. D.; Chandler, D.; Andersen, H. C. Role of repulsive forces in determining the equilibrium structure of simple liquids. *J. Chem. Phys.* **1971**, *54*, 5237–5247.
79 Plimpton, S. Fast parallel algorithms for short-range molecular dynamics. *J. Comput. Phys.* **1995**, *117*, 1–19.
80 Lammps version: October 03, 2020. available at: http:/lammps. sandia. gov.
81 Xu, W. S.; Douglas, J. F.; Freed, K. F. Influence of cohesive energy on the thermodynamic properties of a model glass-forming polymer melt. *Macromolecules* **2016**, *49*, 8341–8354.
82 De Gennes, P. G. *Scaling Concepts in Polymer Physics*. Cornell University Press: Ithaca, New York, **1979**.
83 Wittmer, J. P.; Beckrich, P.; Johner, A.; Semenov, A. N.; Obukhov, S. P.; Meyer, H.; Baschnagel, J. Why polymer chains in a melt are not random walks. *Europhys. Lett.* **2007**, *77*, 56003.
84 Wittmer, J. P.; Beckrich, P.; Meyer, H.; Cavallo, A.; Johner, A.; Baschnagel, J. Intramolecular long-range correlations in polymer melts: the segmental size distribution and its moments. *Phys. Rev. E* **2007**, *76*, 011803.
85 Allen, M. P.; Tildesley, D. J. *Computer simulation of liquids*. Oxford University Press: **1987**.
86 Xu, W. S.; Douglas, J. F.; Xu, X. Molecular dynamics study of glass formation in polymer melts with varying chain stiffness. *Macromolecules* **2020**, *53*, 4796–4809.
87 Xu, W. S.; Douglas, J. F.; Xia, W.; Xu, X. Investigation of the temperature dependence of activation volume in glass-forming polymer melts under variable pressure conditions. *Macromolecules* **2020**, *53*, 6828–6841.
88 Xu, W. S.; Douglas, J. F.; Xu, X. Role of cohesive energy in glass formation of polymers with and without bending constraints. *Macromolecules* **2020**, *53*, 9678–9697.
89 Xu, X.; Douglas, J. F.; Xu, W. S. Influence of side-chain length and relative rigidities of backbone and side chains on glass formation of branched polymers. *Macromolecules* **2021**, *54*, 6327–6341.
90 Douglas, J. F.; Xu, W. S. Equation of state and entropy theory approach to thermodynamic scaling in polymeric glass-forming liquids. *Macromolecules* **2021**, *54*, 3247–3269.
91 Yang, Z.; Xu, X.; Xu, W. S. Influence of ionic interaction strength on glass formation of an ion-containing polymer melt. *Macromolecules* **2021**, *54*, 9587–9601.
92 Xu, X.; Xu, W. S. Melt properties and string model description of glass formation in graft polymers of different side-chain lengths. *Macromolecules* **2022**, *55*, 3221–3235.
93 Pazmiño Betancourt, B. A.; Starr, F. W.; Douglas, J. F. String-like collective motion in the α- and β-relaxation of a coarse-grained polymer melt. *J. Chem. Phys.* **2018**, *148*, 104508.
94 Starr, F. W.; Douglas, J. F.; Sastry, S. The relationship of dynamical heterogeneity to the Adam-Gibbs and random first-order transition theories of glass formation. *J. Chem. Phys.* **2013**, *138*, 12A541.
95 Zhang, H.; Zhong, C.; Douglas, J. F.; Wang, X.; Cao, Q.; Zhang, D.; Jiang, J. Z. Role of string-like collective atomic motion on diffusion and structural relaxation in glass forming Cu-Zr alloys. *J. Chem. Phys.* **2015**, *142*, 164506.
96 Kincaid, J. F.; Eyring, H.; Stearn, A. E. The theory of absolute reaction rates and its application to viscosity and diffusion in the liquid state. *Chem. Rev.* **1941**, *28*, 301–365.
97 Glasstone, S.; Laidler, K. J.; Eyring, H. *The Theory of Rate Processes: The Kinetics of Chemical Reactions, Viscosity, Diffusion and Electrochemical Phenomena*. McGraw-Hill Book Company, Incorporated: **1941**.
98 Xu, W.-S.; Douglas, J. F.; Freed, K. F. Stringlike cooperative motion explains the influence of pressure on relaxation in a model glass-forming polymer melt. *ACS Macro Lett.* **2016**, *5*, 1375–1380.
99 Xu, W.-S.; Douglas, J. F.; Freed, K. F. Influence of cohesive energy on relaxation in a model glass-forming polymer melt. *Macromolecules* **2016**, *49*, 8355–8370.
100 Vogel, H. The law of the relation between the viscosity of liquids and the temperature. *Phys. Z.* **1921**, *22*, 645–646.
101 Fulcher, G. S. Analysis of recent measurements of the viscosity of glasses. *J. Am. Ceram. Soc.* **1925**, *8*, 339–355.
102 Tammann, G.; Hesse, W. Die Abhängigkeit der Viscosität von der Temperatur bie unterkühlten Flüssigkeiten. *Z. Anorg. Allg. Chem.* **1926**, *156*, 245–257.
103 Hanakata, P. Z.; Douglas, J. F.; Starr, F. W. Interfacial mobility scale determines the scale of collective motion and relaxation rate in polymer films. *Nat. Commun.* **2014**, *5*, 4163.
104 Pazmiño Betancourt, B. A.; Hanakata, P. Z.; Starr, F. W.; Douglas, J. F. Quantitative relations between cooperative motion, emergent elasticity, and free volume in model glass-forming polymer materials. *Proc. Natl. Acad. Sci. U. S. A.* **2015**, *112*, 2966–2971.
105 Hanakata, P. Z.; Pazmiño Betancourt, B. A.; Douglas, J. F.; Starr, F. W. A unifying framework to quantify the effects of substrate interactions, stiffness, and roughness on the dynamics of thin supported polymer films. *J. Chem. Phys.* **2015**, *142*, 234907.

https://doi.org/10.1007/s10118-023-3004-5

106 Hall, R. W.; Wolynes, P. G. The aperiodic crystal picture and free energy barriers in glasses. *J. Chem. Phys.* **1987**, *86*, 2943–2948.
107 Simmons, D. S.; Cicerone, M. T.; Zhong, Q.; Tyagi, M.; Douglas, J. F. Generalized localization model of relaxation in glass-forming liquids. *Soft Matter* **2012**, *8*, 11455–11461.
108 Götze, W. *Complex dynamics of glass-forming liquids: A mode-coupling theory*. Oxford University Press on Demand: **2008**, Vol. 143.
109 Flory, P. J.; Vrij, A. Melting points of linear-chain homologs. the normal paraffin hydrocarbons. *J. Am. Chem. Soc.* **1963**, *85*, 3548–3553.
110 Sokolov, A. P.; Novikov, V. N.; Ding, Y. Why many polymers are so fragile. *J. Phys.: Condens. Matter* **2007**, *19*, 205116.
111 Dalle-Ferrier, C.; Kisliuk, A.; Hong, L.; Carini, G.; Carini, G.; D' Angelo, G.; Alba-Simionesco, C.; Novikov, V. N.; Sokolov, A. P. Why many polymers are so fragile: a new perspective. *J. Chem. Phys.* **2016**, *145*, 154901.
112 Xu, W. S.; Freed, K. F. Generalized entropy theory of glass formation in polymer melts with specific interactions. *Macromolecules* **2015**, *48*, 2333–2343.
113 Xu, W. S.; Freed, K. F. Influence of cohesive energy and chain stiffness on polymer glass formation. *Macromolecules* **2014**, *47*, 6990–6997.
114 Ruan, D.; Simmons, D. S. Glass formation near covalently grafted interfaces: ionomers as a model case. *Macromolecules* **2015**, *48*, 2313–2323.
115 Xu, W. S.; Douglas, J. F.; Freed, K. F. Influence of pressure on glass formation in a simulated polymer melt. *Macromolecules* **2017**, *50*, 2585–2598.
116 Zhang, W.; Starr, F. W.; Douglas, J. F. Collective motion in the interfacial and interior regions of supported polymer films and its relation to relaxation. *J. Phys. Chem. B* **2019**, *123*, 5935–5941.
117 Fan, J.; Emamy, H.; Chremos, A.; Douglas, J. F.; Starr, F. W. Dynamic heterogeneity and collective motion in star polymer melts. *J. Chem. Phys.* **2020**, *152*, 054904.
118 Aichele, M.; Gebremichael, Y.; Starr, F. W.; Baschnagel, J.; Glotzer, S. C. Polymer-specific effects of bulk relaxation and stringlike correlated motion in the dynamics of a supercooled polymer melt. *J. Chem. Phys.* **2003**, *119*, 5290–5304.
119 Gebremichael, Y.; Schrøder, T. B.; Starr, F. W.; Glotzer, S. C. Spatially correlated dynamics in a simulated glass-forming polymer melt: analysis of clustering phenomena. *Phys. Rev. E* **2001**, *64*, 051503.
120 Hung, J. H.; Simmons, D. S. Do string-like cooperative motions predict relaxation times in glass-forming liquids. *J. Phys. Chem. B* **2020**, *124*, 266–276.
121 Kauzmann, W.; Eyring, H. The viscous flow of large molecules. *J. Am. Chem. Soc.* **1940**, *62*, 3113–3125.
122 Jeong, C.; Douglas, J. F. Mass dependence of the activation enthalpy and entropy of unentangled linear alkane chains. *J. Chem. Phys.* **2015**, *143*, 144905.

https://doi.org/10.1007/s10118-023-3004-5